ACS OMEGA

http://pubs.acs.org/journal/acsodf

Article

Li-Doped Ti Surface for the Improvement of Osteointegration

Longhai Qiu, Zhanbei Zhu, Feng Peng,* Chi Zhang, Juning Xie, Ruixiang Zhou, Yu Zhang,* and Mei Li*

Cite This: *ACS Omega* 2022, 7, 12030−12038

Read Online

ACCESS | Metrics & More | Article Recommendations | Supporting Information

ABSTRACT: Aseptic loosening is the main factor that leads to the failure of orthopedic implants. Enhancing the early osteointegration of a bone implant can lower the risk of aseptic loosening. Here, a Li-doped surface was constructed on a Ti surface via plasma electrolytic oxidation (PEO) to improve osteointegration. The prepared Li-doped PEO coating showed a porous morphology and the sustained release of Li ions. *In vitro* results of rat bone marrow mesenchymal stem cell (rBMSC) culture studies suggested that the Li-doped Ti surface significantly favored cell adhesion. Moreover, it was found that the Li-doped surface enhanced alkaline phosphatase activity and extracellular matrix mineralization of rBMSCs. In addition, the surface improved the expression of osteogenesis-related genes. Furthermore, a bone implantation model indicated that the Li-doped Ti surface showed improved osteointegration. The incorporation of Li into a Ti surface is a promising method for orthopedic applications.

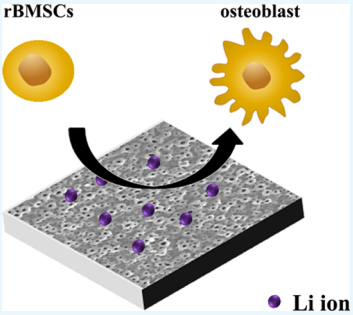

1. INTRODUCTION

The use of orthopedic implants has dramatically increased in the past few years as a result of population aging and patients' quest for a better quality of life.[1] Titanium (Ti) is an inert metal with good biocompatibility, reliable mechanical properties, and corrosion resistance; thus, it is a commonly used biological material for orthopedic implants. Ti and its alloys are widely used as bone plates, bone nets, and scaffolds. For example, screw-type Ti-based implants have achieved a good clinical result.[2−5] However, the loosening and the failure of implants still occur in cases of osteoporosis, periodontitis, rheumatoid arthritis, and diabetes. These were mainly because the inert Ti surface provides inadequate osseointegration.[6] Studies have shown that aseptic loosening occurred in 51.9% of patients that failed prosthesis after total hip arthroplasty.[7] Therefore, the ability of titanium-based implants for osseointegration has to be improved. This is a major challenge in the long-term success of titanium-based implants.[8,9]

Surface modification technologies such as plasma electrolytic oxidation (PEO), spray coating, and plasma immersion ion implantation have been applied on Ti surfaces to alter their topological morphology and phase composition and thus to improve their biological performances.[4,10−12] In particular, PEO has been considered as an economical and effective electrochemical surface modification method, which can produce surfaces with porous structures and alterative compositions.[13] By changing the composition of electrolytes, the PEO coating can be loaded with various bioactive ions such as argentum (Ag), calcium (Ca), and strontium (Sr).[5,14,15] These bioactive ions play curial roles in the behavior of cells with bones. For example, Ca participates in autophagic mTOR and AMPK signaling pathways, thus enhancing the mineralization of osteoblasts.[16]

Lithium (Li) is a non-essential micronutrient, which has been used in medicine and the treatment of bipolar disorders for a long time.[17] Li has been also found to have other biological effects including the inhibition of osteoclast formation and osteolysis, alleviation of cartilage degeneration, and promotion of cartilage regeneration.[18,19] Recently, a few studies have found that Li modulates the glycogen synthase kinase-3β and the typical Wnt signal of bone-related cells; thus, Li plays an important role in the balance between bone metabolism and formation.[20,21] Furthermore, Li has been shown to regulate the polarization of macrophages through the PI3K/AKT signal axis, thus achieving good immune regulation in the process of bone integration.[22] Meanwhile, Li also produces anti-inflammatory effects. Its neuroprotective effect is gradually realized through anti-neuritis. It reduces the levels of IL-1 β in the frontal cortex and hippocampus of rats and TNF α in the hippocampus of rats.[23] In addition, Li-doped scaffolds have been reported to support the regeneration of articular cartilage defects, which stimulated the secretion of MIR-130A derived from bone marrow stromal cells and promoted angiogenesis.[24,25] Based on the above-mentioned research, we have considered that Li most likely has direct effects on osteogenesis.

Here, we prepared Li-containing PEO coatings for Ti to improve the osteogenic properties. The osteogenic performances of Li-doped PEO coatings were studied both *in vitro* and *in vivo*.

Received: January 11, 2022
Accepted: March 24, 2022
Published: April 3, 2022

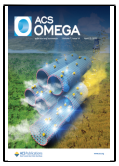

© 2022 The Authors. Published by American Chemical Society

https://doi.org/10.1021/acsomega.2c00229
ACS Omega 2022, 7, 12030−12038

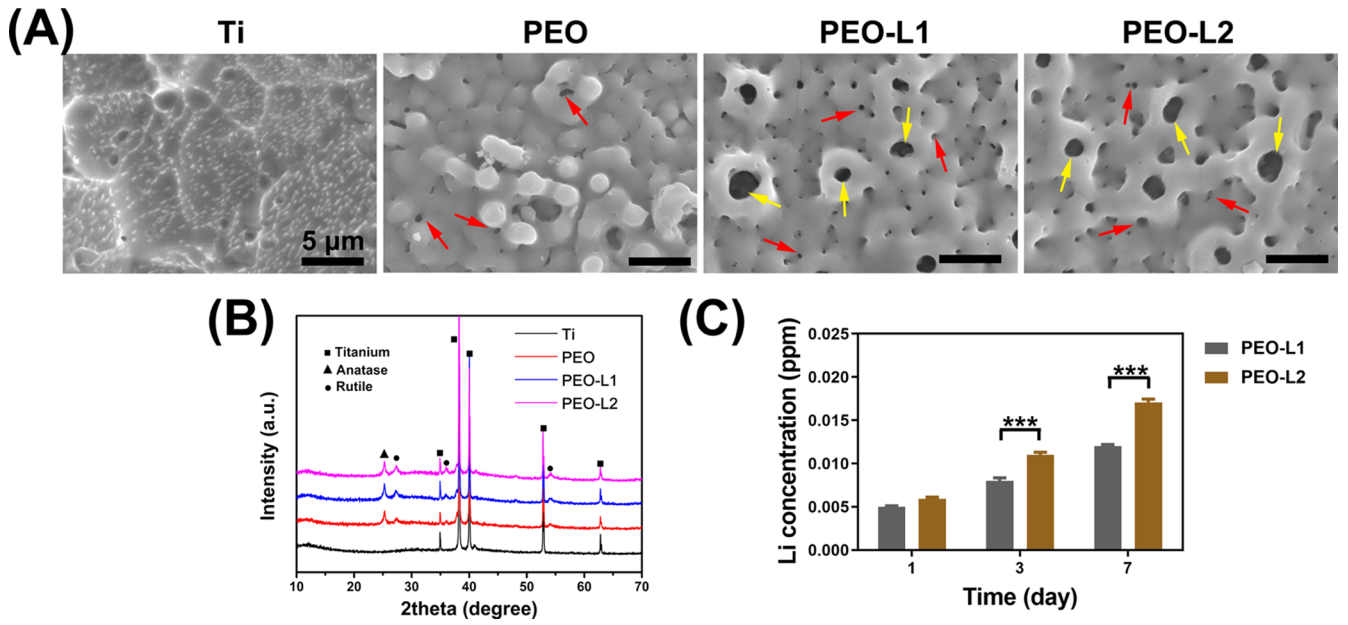

Figure 1. Surface views (A) and XRD patterns (B) of Ti, PEO, PEO-L1, and PEO-L2 samples; red arrows indicate small pores on the PEO-coated surface, and yellow arrows indicate large pores on the PEO-coated surfaces; accumulation of released Li ions from PEO-L1 and PEOL-L2 samples immersed in deionized water (C).

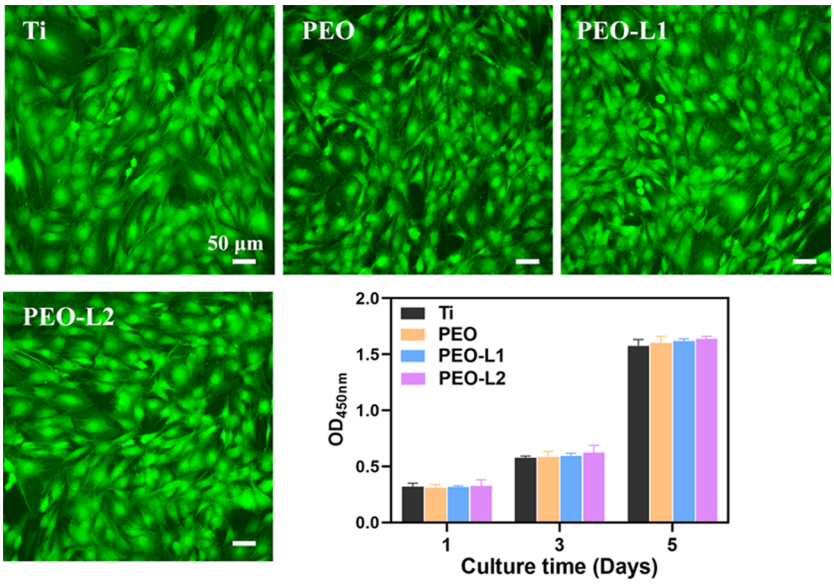

Figure 2. Live/dead staining of rBMSCs cultured on Ti, PEO, PEO-L1, and PEO-L2 samples for 3 days. CCK8 assay for the proliferation of BMSCs cultured on Ti, PEO, PEO-L1, and PEO-L2 samples for 1, 3, and 5 days.

2. RESULTS AND DISCUSSION

PEO is a commonly used surface treatment technology, which improves the biological performance of a Ti implant.[10,26,27] Recent studies have revealed that Li has a positive influence on immune regulation for osteointegration and induces exosome secretion that promotes angiogenesis.[22,24] In this study, we studied the direct influence of Li-doped PEO-coated Ti on rat bone marrow mesenchymal stem cells (rBMSCs). Surface views of various prepared samples are shown in Figure 1a. After PEO treatment, all the samples exhibited a rough surface with volcanic shapes. Small pores (indicated by red arrows) with diameters of 0.3−0.6 μm were uniformly distributed on the surface of the PEO sample. However, large pores (indicated by yellow arrows) with diameters of 1−2 μm were also observed in PEO-L1 and PEO-L2 samples. This may be caused by the increase in conductivity of the electrolyte after introduction of Li ions. The size of cell is 20−100 μm; therefore, the pores most likely have minimal influences on the cell behaviors.

X-ray diffraction (XRD) patterns of various prepared samples are shown in Figure 1b. Ti feature peaks were detected only for uncoated Ti samples. All PEO-coated samples showed similar feature peaks with both anatase (25.37, 37.88, 48.12, and 55.1°) and rutile TiO_2 (27.48, 36.13, and 54.37°) detected. The product of the PEO-treated sample is mainly metal oxides. The temperature near the sample can be over 2000 °C.[28] Anatase TiO_2 can be transferred to rutile TiO_2 at 915 °C; thus, both types of TiO_2 were detected in the

https://doi.org/10.1021/acsomega.2c00229
ACS Omega 2022, 7, 12030−12038

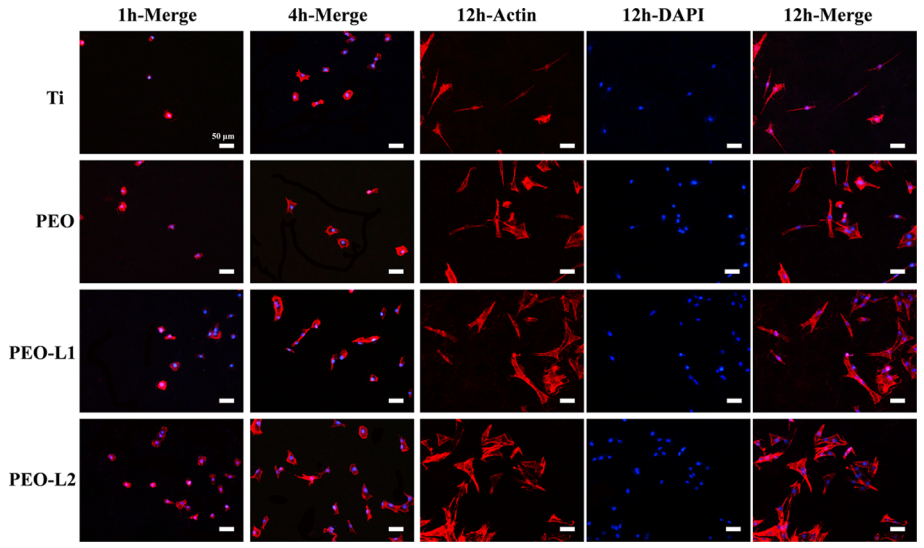

Figure 3. Cytoskeleton staining of rBMSCs cultured on Ti, PEO, PEO-L1, and PEO-L2 samples for 1, 4, and 12 h. The F-actin and nucleus were stained by rhodamine phalloidin (red) and DAPI (blue), respectively.

PEO-treated Ti samples. Element Li is too light to be detected by energy dispersive spectrometry and X-ray photoelectron spectroscopy technologies. Nevertheless, other studies have shown that elements in the electrolyte are evenly distributed on PEO coatings.[29,30] Moreover, we investigated the accumulation of Li ions released from various samples. Significantly, more Li ions were released from the PEO-L2 sample after incubation in deionized water for 3 and 7 days, as shown in Figure 1c. More Li ions in the electrolyte of PEO-L2 resulted in more Li elements incorporated into the coating; thus, more Li ions were released from the PEO-L2 sample.

The cytocompatibility of Ti, PEO, PEO-L1, and PEO-L2 samples was determined using a standard CCK-8 assay and live/dead staining (Figure 2). In general, the amount of formazan dye generated by dehydrogenases in the viable cell sample is directly proportional to the number of living cells in the CCK-8 assay. Our results suggested that there was no significant difference in the number of viable cells among the four sample groups. The cells exhibited increased viability in the samples when the incubation time was increased. The collected live/dead cell staining images indicated that there were no obvious dead cells (red fluorescence) adhered on different samples. Typical stem cell forms were found and spread out in a healthy manner (green fluorescence) on the sample surfaces. Thus, the use of Li preserved the cytocompatibility of rBMSCs on the titanium substrate. To further investigate the cytoskeletal organization on various surfaces, rBMSCs were stained with rhodamine phalloidin and 4′,6-diamidino-2-phenylindole (DAPI). The cytoskeletal organization and cell densities on each sample are shown in Figure 3. A slight difference after incubation for 1, 4, and 24 h was observed. The rBMSCs on PEO-L2 displayed good adhesion and high cell density (Figure 3) and spreading area (Figure S1). Moreover, the cellular pseudopodia of the rBMSCs on the PEO-L2 coating extended earlier, and their filopodia extensions were more developed than in other coatings. Furthermore, the mutual cross-linked cells on the PEO-L2 coating showed that the cells were tightly connected. Moreover, the cells cultured on PEO-L2 showed significantly higher expression of genes, including vinculin and paxillin, than the other three samples (Figure S2), which indicated that PEO-L2 was more beneficial for the recruitment of BMSCs. Our results validated that the introduction of Li into the PEO coating provided a more suitable environment for rBMSC adhesion and growth. This confirms the good biocompatibility of Li to osteogenesis-related cells, which is consistent with previous research studies.[31,32]

Alkaline phosphatase (ALP) is a byproduct of osteoblast activity, which has been considered to be an early indicator of osteogenic differentiation; thus, an elevated ALP is an indication of active bone formation.[33,34] Therefore, the ALP activity was measured at 7 and 14 days to investigate the osteogenic differentiation potential of rBMSCs that were cultured on the samples. An ALP staining kit that provided a quick and easy method to stain ALP in stem cells was used with 5-bromo-4-chloro-3-indolyl phosphate (BCIP) as the substrate, and ALP staining is based on the ability of ALP to hydrolyze the phosphate group on BCIP to produce blue-colored intermediates, which are then oxidized by nitro blue tetrazolium (NBT) to form an insoluble dark- or purple−blue NBT formazan.[35] As shown in Figure 4A, the PEO coating with Li displayed denser and deeper ALP positive staining after 7 and 14 days of induction. The staining results for Ti and PEO groups were similar. Meanwhile, *para*-nitrophenyl phosphate (*p*-NPP) is also a commonly used phosphatase chromogenic substrate, which can be catalyzed by ALP to generate yellow *p*-NP under alkaline conditions. Based on this, the level of ALP activity can be quantitatively calculated by colorimetric analysis using a *p*-NP standard curve alignment. Our quantitative results of ALP activity levels (U/mg) revealed that coatings with Li were favorable for elevating the ALP activity at days 7 and 14 compared to the other two groups ($p < 0.01$, Figure 4B). The activity levels showed the trend of Ti < PEO < PEO-L1 < PEO-L2. As the final stage of osteogenic differentiation, matrix mineralization was mainly mediated by osteoblasts that secrete mineral precursors, including calcium- and phosphate-rich materials.[36] When the rBMSCs were cultured with ascorbic acid, phosphate, and dexamethasone for 14 days, extracellular calcified nodules formed on the sample surfaces. These were visualized by alizarin red (AR) S staining. Using a stereomicroscope, we confirmed that a calcium matrix was successfully deposited on the PEO-

https://doi.org/10.1021/acsomega.2c00229
ACS Omega 2022, 7, 12030−12038

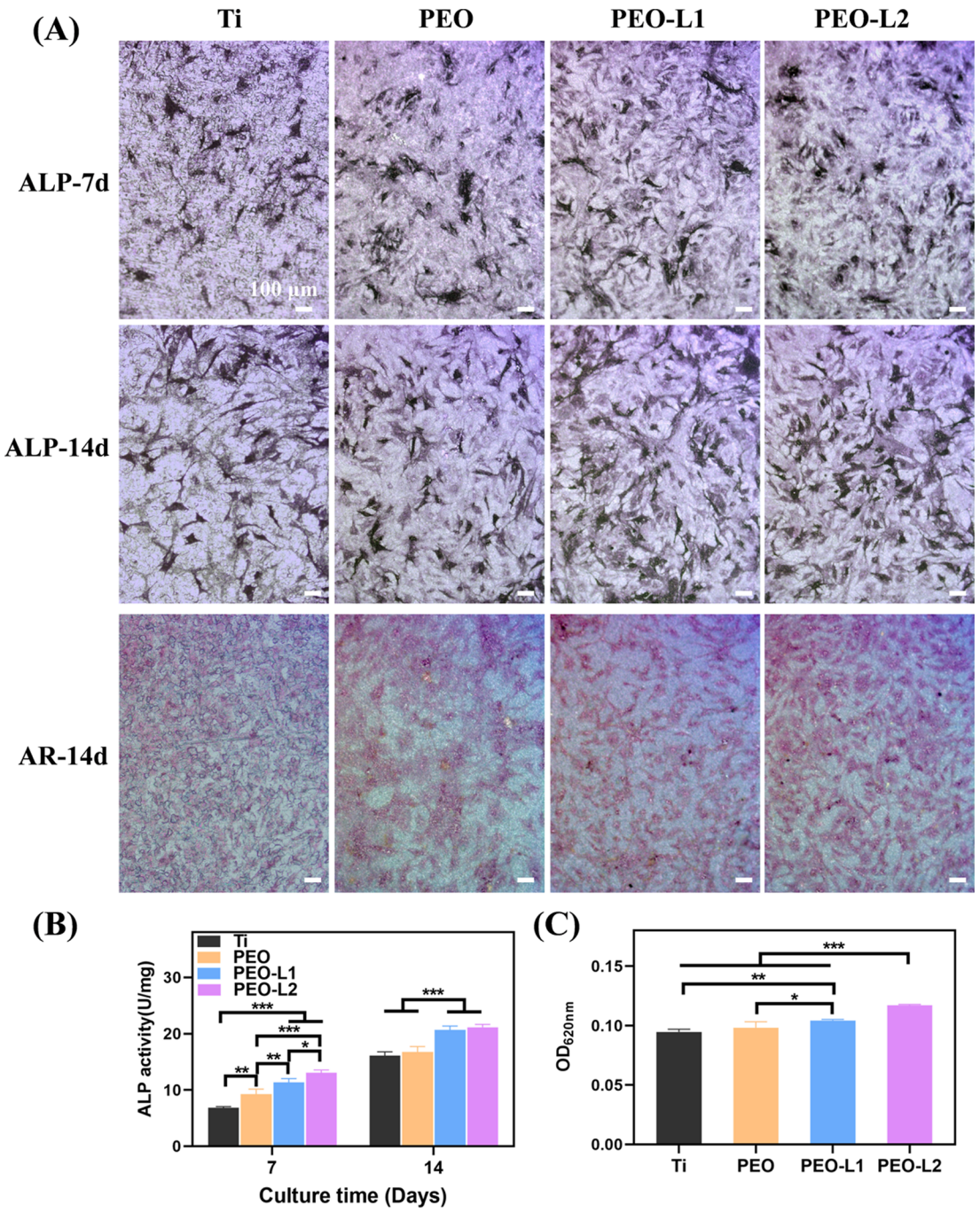

Figure 4. Representative ALP staining and ARS staining images of rBMSCs cultured on different samples (A). Quantitative analysis of the ALP activity (B) and ECM mineralization (C).

modified surface. This was pronounced in the PEO-L2 group, while the trends among the four groups were consistent with ALP results. The relative quantitation results in Figure 4C showed that the formation of mineralized nodules is 1.2 times greater in PEO-L2 than in the Ti and PEO groups. These results revealed that Li-incorporated samples were beneficial for osteogenic differentiation of rBMSCs especially PEO-L2. Although previous studies have shown that Li therapy enhances bone anabolism and increases bone mineral density in mice,[37] our material preparation was simple and more suitable for orthopedics. The local release of Li from the surface coating could promote osteogenic differentiation of stem cells and accelerate bone repair while reducing the side effects of systemic Li use.

The expression of osteogenic-related markers in rBMSCs after incubation on different samples for 7 and 14 days was detected by real-time polymerase chain reaction (RT-PCR) assay. The results were calculated by normalizing to a housekeeping gene and expressing as relative levels to the Ti group (Figure 5). The tested genes included two early osteoblast markers [runt-related transcription factor 2 (Runx2) and ALP] and two late markers [osteocalcin (OCN) and collagen I (COL I)]. Runx2 is the main transcription factor. The activation of Runx2 commits cells to osteogenic lineage.[38] In addition, Runx2 combines with a

https://doi.org/10.1021/acsomega.2c00229
ACS Omega 2022, 7, 12030−12038

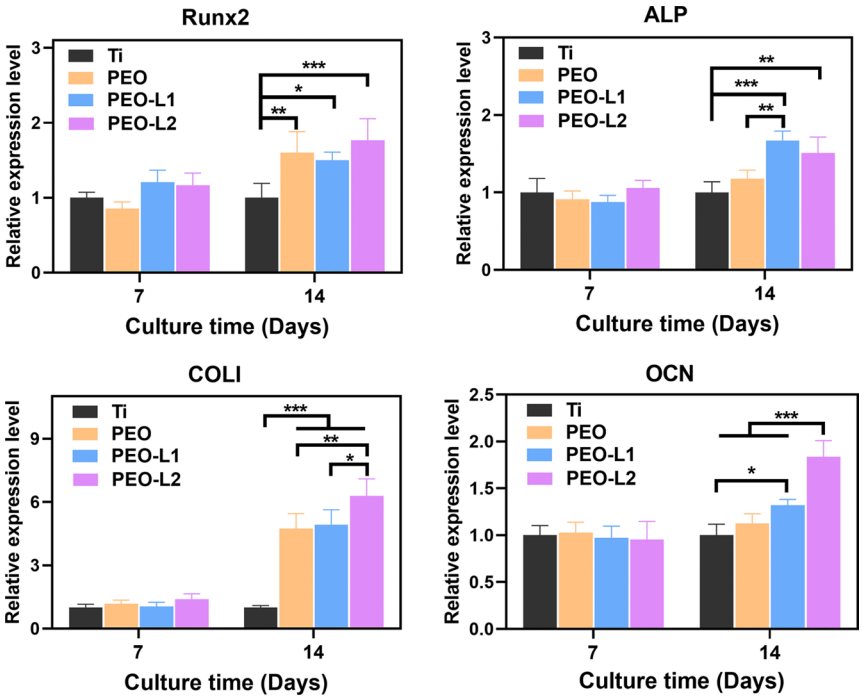

Figure 5. Relative mRNA expression of osteogenesis markers Runx2, ALP, OPN, and OCN of the rBMSCs cultured on Ti, PEO, PEO-L1, and PEO-L2 samples with osteogenic differentiation for 7 and 14 days.

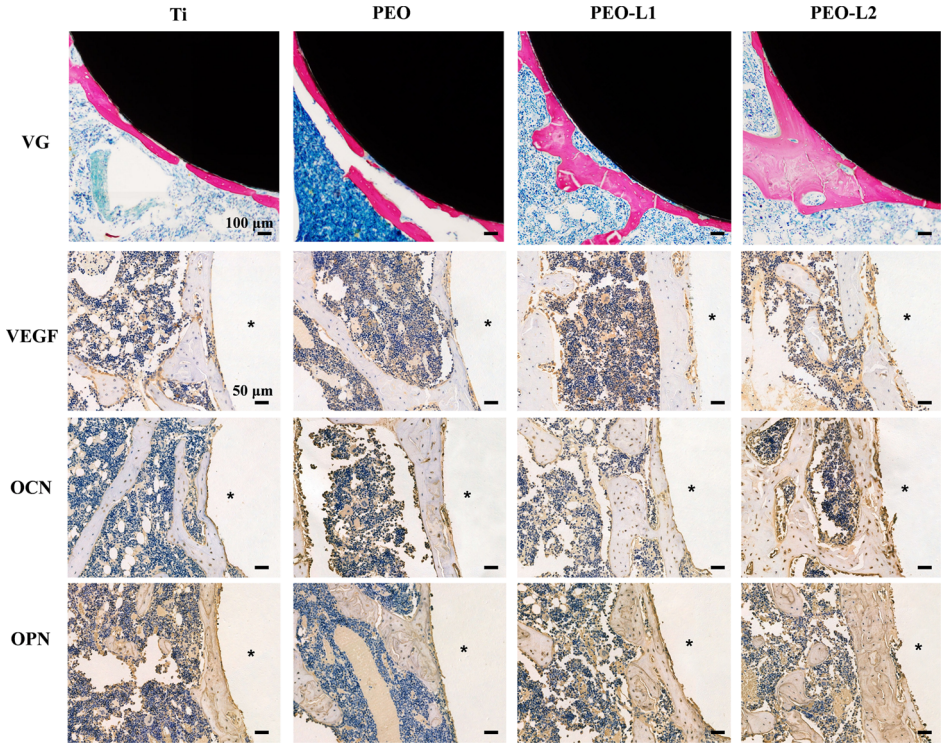

Figure 6. Representative VG staining images of undecalcified femur sections with Ti, PEO, PEO-L1, and PEO-L2 pillars at an implantation time of 8 weeks. Representative immunohistochemical images of OPN, OCN, and VEGF staining of decalcified sections after 8 weeks. The asterisk symbols show implants.

core-binding factor subunit to form a heterodimer. This regulated OCN, OPN, bone sialoprotein, and many others. Runx2 deletion *in vivo* could result in complete osteoblast absence.[39] Therefore, Runx2 expression during early skeletal development is essential for osteoblast differentiation. Meanwhile, COL I and OCN are the two most abundant proteins during bone growth.[40] As shown in Figure 5, the cells cultured on PEO-L2 samples showed the highest expression of Runx2, COL I, and OCN compared with other groups at day 14. The relative expression levels of COL I and OCN in the PEO-L2 group were 6.2- and 1.8-fold higher than those in the control group (Ti), respectively. These data implied that the enhanced

https://doi.org/10.1021/acsomega.2c00229
ACS Omega 2022, 7, 12030−12038

osteogenic differentiation was due to the regulatory effects of released Li on osteogenesis-related genes. In addition, Li has been reported to modulate intracellular signaling pathways that are related to bone repair, such as glycogen synthase kinase-3β and wnt/β-catenin signaling.[21,37,41,42]

Our *in vitro* experiments confirmed that osteogenic induction was dependent on Li doping. To further examine the osteointegration capacity *in vivo*, a bone-implant model was used. Li-coated pillars were employed as implants in rat femurs. At week 8 post implantation with the coated pillars, the bone tissues with implants were harvested. The bone around implants was stained red through Van Gieson's (VG) staining for undecalcified sections. As shown in Figure 6, there were only a few new bone tissues surrounding the Ti implant. The bone tissues were not bound tightly to Ti. By contrast, completed new bone circles were formed in Li-incorporated pillars. The new bones in PEO-L1 and PEO-L2 groups were more connected and thicker than those in other groups. The bone-implant contact ratio revealed the same trend (Figure S3). The special markers (OCN and OPN) of osseointegration were immunohistochemically stained on decalcified histological sections. After 8 weeks, larger stained areas and deeper positive staining were observed around the coated implants than the uncoated Ti implant. Notably, PEO-L1 and PEO-L2 groups exhibited most OCN and OPN expression around the implants during bone reconstitution. OPN is not only an important bone matrix protein and closely related to bone formation and development[43−45] but also plays an important regulatory role in vascular remodeling.[46,47] Our Li-incorporated implants also enhanced the expression of the pro-angiogenic factor (VEGF), which contributed to the construction of a pro-angiogenic biochemical microenvironment.[24] Therefore, our results confirmed that the release of Li ions from the implants effectively promoted the osseointegration *in vivo*.

3. CONCLUSIONS

We introduced Li into Ti surfaces via PEO treatment. The modified Ti implants showed sustained release of Li ions. Li-doped Ti surfaces favored osteogenesis differentiation behaviors of rBSMCs. The in vivo experiments also demonstrated that the developed implant provided superior osteointegration than uncoated Ti. Our findings suggest that the Li-modified surface on Ti is a promising strategy for orthopedic implants.

4. MATERIALS AND METHODS

4.1. Synthesis and Characterization of Li-Doped PEO Coating on Ti. Ti specimens were cut into 10 × 10 × 1 mm and ϕ 2 mm × 8 mm for *in vitro* and *in vivo* assays, respectively. The PEO process was conducted in electrolyte solution containing 0.05 M $NaSiO_3$, 0.1 M KOH, and X M $LiCH_3COO$ (X = 0, 0.01, and 0.05) at a current of 0.8 A for 3 min. The obtained samples were denoted as Ti, PEO, PEO-L1, and PEO-L2, respectively. Afterward, all samples were sterilized using ethylene oxide for 6 h at 55 °C.

The surface views and surface phase compositions were analyzed using a scanning electron microscope (S-3400N, Hitachi, Japan) and XRD (d8 ADVANCE, Bruker, Germany), respectively.

4.2. Ion Release. The samples were immersed in 10 mL of deionized water. Liquid samples were collected after 1, 3, 5, and 7 days. To each collected sample, 10 mL of deionized water was added. The Li ion concentration was determined using inductively coupled plasma atomic emission spectroscopy (iCAP RQ, Thermo Fisher Scientific, USA).

4.3. Cell Culture. rBMSCs were purchased from Cyagen Biosciences. The cells were cultured in Dulbecco's modified Eagle's medium/F12 medium (Gibco, USA) supplemented with 10% fetal bovine serum (Gibco) and 1% penicillin/streptomycin at 37 °C in a humid atmosphere of 5% CO_2. The culture medium was exchanged every 48 h.

4.4. Cell Adhesion. rBMSCs (2×10^3 cells/well) were seeded on Ti, PEO, PEO-L1, and PEO-L2 samples in 24-well plates. After 1, 4, and 12 h of incubation, the samples were washed twice with phosphate buffered saline (PBS), fixed in 4% paraformaldehyde for 15 min at room temperature, and then permeabilized with 0.1% Triton X-100 for 2 min. The actin cytoskeleton of the cells was stained with phalloidin rhodamine (Sigma, USA) for 1 h. The nuclei were counterstained with DAPI (Sigma, USA) for 15 min. Finally, the samples were imaged using a fluorescence microscope (Olympus IX 71, Olympus, Japan).

4.5. Cell Proliferation and Viability. The rBMSCs (1×10^4 cells/well) were cultured on different samples. Cell proliferation was analyzed using a CCK-8 (DOJINDO, Japan) assay after 1, 3, and 5 days of incubation according to the manufacturer's instructions. The absorbance of the culture medium was measured at 450 nm by using a microplate reader. Cell viability was detected by live/dead staining after 24 h. Briefly, the samples were washed using PBS. Live and dead cells on the samples were stained with calcein-AM (2 μM) and propidium iodide (PI, 5 μM), respectively, for 15 min at 37 °C. Finally, the cell viability was then observed by fluorescence microscopy.

4.6. ALP Activity Assay. The rBMSCs (5×10^3) were seeded on different samples in 24-well plates. After 24 h, osteogenic differentiation of cells was induced by culture medium supplemented with 50 μg/mL ascorbic acid, 10 mM β-glycerophosphate, and 10 nM dexamethasone. At days 7 and 14, the cells were stained using the BCIP/NBT ALP Chromogenic Kit (Beyotime Biotechnology, China). Intracellular ALP catalyzes the BCIP/NBT substrate to form an insoluble formazan. The level of enzyme activity was determined by the substrate color. Meanwhile, after osteogenic induction, the intracellular total protein concentration was measured using the BCA protein assay kit (Pierce, Thermo Fisher Scientific, USA). The intracellular ALP was measured using the ALP assay kit (Beyotime Biotechnology, China). The enzyme activity (U/mg) was then calculated by normalizing ALP to the protein content.

4.7. Extracellular Matrix Mineralization Assay. The cells were cultured on different samples, and osteoblast growth was induced for 14 days as described above. The resulting cells were then stained with AR (40 mM). The staining images of extracellular matrix mineralization (ECM) were observed using a phase-contrast inverted optical microscope (Olympus, Japan). For quantitative analysis, the bonded dye was quantified by dissolving in 10% cetylpyridinium chloride (Sigma-Aldrich, USA), and the OD_{620} values were measured using a microplate reader.

4.8. Real-Time Polymerase Chain Reaction. The rBMSCs (1×10^5) were seeded on different samples for 24 h and then cultured with osteogenic differentiation medium for 7 and 14 days. Total RNA was extracted by using the TRIzol

https://doi.org/10.1021/acsomega.2c00229
ACS Omega 2022, 7, 12030−12038

reagent (Invitrogen, USA). Then, 500 ng of total RNA was used to synthesize complementary DNA (cDNA) by using EasyScript All-in-One First-Strand cDNA Synthesis SuperMix for qPCR (Trans, China). Finally, PerfectStart Green qPCR SuperMix (Trans, China) was applied to quantitatively analyze osteogenesis-related genes, including ALP, Runx2, COL-I, and OCN. GAPDH was the housekeeping gene. All the primer sequences used in this study are presented in Table S1.

4.9. Bone Implantation. Twenty male Sprague-Dawley rats weighing 240−250 g were purchased from the Medical Experimental Animal Center of Guangdong Province. The animals were randomly divided into Ti, PEO, PEO-L1, and PEO-L2 groups. All the procedures in the animal experiments were approved by the Guidelines for Care and Use of Laboratory Animals of South China University of Technology and the Animal Ethics Committee of Guangdong Provincial People's Hospital (KY-Z-2021-381-01). Before surgery, animals were shaved, and the surgical site was disinfected. After anesthetization, an incision was made around the knee, which exposed the lateral femoral condyle. A 2 mm-diameter hole was made by using a drill through the lateral femoral condyles (Figure S4). The cylinder sample (2 mm in diameter, 5 mm in length) was pressed fit into the hole, and then, the wound was disinfected and gently closed. 8 weeks after surgery, all animals were sacrificed by an overdose of pentobarbitone. The femurs with implants were collected and fixed in 4% paraformaldehyde. After gradient dehydration and embedding in polymethylmethacrylate, tissues were cut into sections by using a saw microtome (EXAKT Apparatebau, Germany). Then, VG staining was performed on the sections polished to about 50 μm, and the representative pictures were acquired using a microscope (Olympus, Japan). The osseous tissues were decalcified in EDTA decalcifying solution for 4 weeks, and then, the implants were removed gently from the femurs. The decalcified femurs were then dehydrated, embedded, and then cut into 5 μm-thick slices. Afterward, the obtained sections were dewaxed in xylene and hydrated in gradient ethanol. Through antigen retrieval and blocking, the sections were incubated with primary antibodies (VEGF, OCN, OPN; Servicebio, China) and the goat anti-rabbit IgG secondary antibody (InvivoGen, USA). Finally, the positive protein expression was detected by 3,3′-diaminobenzidine solution (Dako, Denmark) and the hematoxylin counterstaining process and examined using a microscope.

4.10. Statistical Analysis. Mean ± standard deviation is presented from repeated independent experiments. Differences among groups were analyzed with two-way analysis of variance followed by the SNK test using SPSS20.0 software. Statistical significance was confirmed when the P-value is less than 0.05 ($^*P < 0.05$, $^{**}P < 0.01$, $^{***}P < 0.001$).

■ ASSOCIATED CONTENT

Supporting Information

The Supporting Information is available free of charge at https://pubs.acs.org/doi/10.1021/acsomega.2c00229.

Primer sequences used for RT-PCR amplification; spreading area of BMSCs cultured on Ti, PEO, PEO-L1, and PEO-L2 samples for various times; relative mRNA expression of adhesion markers in rBMSCs cultured on Ti, PEO, PEO-L1, and PEO-L2 samples 24 h; bone-implant contact ration of implant samples from the perspective of histopathology after implantation for 4 and 8 weeks; and surgery images and procedure of bone implantation (PDF)

■ AUTHOR INFORMATION

Corresponding Authors

Feng Peng − *Medical Research Center, Department of Orthopedics, Guangdong Provincial People's Hospital, Guangdong Academy of Medical Sciences, Guangzhou 510080, China;* orcid.org/0000-0003-2366-2253; Phone: 86-18616936841; Email: pengfeng@gdph.org.cn

Yu Zhang − *The Second School of Clinical Medicine, Southern Medical University, Guangzhou 510515, China; Medical Research Center, Department of Orthopedics, Guangdong Provincial People's Hospital, Guangdong Academy of Medical Sciences, Guangzhou 510080, China*; Phone: 86-13602744495; Email: zhangyu@gdph.org.cn

Mei Li − *Medical Research Center, Department of Orthopedics, Guangdong Provincial People's Hospital, Guangdong Academy of Medical Sciences, Guangzhou 510080, China;* orcid.org/0000-0002-9265-8541; Phone: 86-15913134863; Email: limei@gdph.org.cn

Authors

Longhai Qiu − *The Second School of Clinical Medicine, Southern Medical University, Guangzhou 510515, China; Medical Research Center, Department of Orthopedics, Guangdong Provincial People's Hospital, Guangdong Academy of Medical Sciences, Guangzhou 510080, China; Department of Traumatology and Orthopaedic Surgery, Institute of Orthopaedics, Huizhou Municipal Central Hospital, Huizhou, Guangdong 516001, China*

Zhanbei Zhu − *Medical Research Center, Department of Orthopedics, Guangdong Provincial People's Hospital, Guangdong Academy of Medical Sciences, Guangzhou 510080, China*

Chi Zhang − *Medical Research Center, Department of Orthopedics, Guangdong Provincial People's Hospital, Guangdong Academy of Medical Sciences, Guangzhou 510080, China*

Juning Xie − *Medical Research Center, Department of Orthopedics, Guangdong Provincial People's Hospital, Guangdong Academy of Medical Sciences, Guangzhou 510080, China*

Ruixiang Zhou − *Medical Research Center, Department of Orthopedics, Guangdong Provincial People's Hospital, Guangdong Academy of Medical Sciences, Guangzhou 510080, China*

Complete contact information is available at: https://pubs.acs.org/10.1021/acsomega.2c00229

Author Contributions

L.Q. and Z.Z. contributed equally to this work. L.Q. and Z.Z.: conceptualization, investigation, methodology, data curation. C.Z., J.X., and R.Z.: supervision, project administration, data curation. F.P., M.L., and Y.Z.: supervision, funding acquisition, review and editing.

Notes

The authors declare no competing financial interest.

■ ACKNOWLEDGMENTS

The Natural Science Foundation of Guangdong Province, China (grant no. 2020A1515011447), Scientific and Techno-

logical Projects of Guangdong Provincial People's Hospital (grant no. 2020bq18), and Scientific and Technological Projects of Guangzhou, China (grant nos. 202002030283, 202102020514, and 201904010376).

REFERENCES

(1) Ige, O. O.; Umoru, L. E.; Aribo, S. Natural Products: A Minefield of Biomaterials. *ISRN Mater. Sci.* **2012**, *2012*, 1−20.
(2) Prasad, K.; Bazaka, O.; Chua, M.; Rochford, M.; Fedrick, L.; Spoor, J.; Symes, R.; Tieppo, M.; Collins, C.; Cao, A.; Markwell, D.; Ostrikov, K. K.; Bazaka, K. Metallic Biomaterials: Current Challenges and Opportunities. *Materials* **2017**, *10*, 884.
(3) Niinomi, M. Metallic biomaterials. *J. Artif. Organs* **2008**, *11*, 105−110.
(4) Xue, T.; Attarilar, S.; Liu, S.; Liu, J.; Song, X.; Li, L.; Zhao, B.; Tang, Y. Surface Modification Techniques of Titanium and its Alloys to Functionally Optimize Their Biomedical Properties: Thematic Review. *Front. Bioeng. Biotechnol.* **2020**, *8*, 603072.
(5) Bai, J.; Wang, H.; Chen, H.; Ge, G.; Wang, M.; Gao, A.; Tong, L.; Xu, Y.; Yang, H.; Pan, G.; Chu, P. K.; Geng, D. Biomimetic osteogenic peptide with mussel adhesion and osteoimmunomodulatory functions to ameliorate interfacial osseointegration under chronic inflammation. *Biomaterials* **2020**, *255*, 120197.
(6) Siddiqi, A.; Payne, A. G. T.; De Silva, R. K.; Duncan, W. J. Titanium allergy: could it affect dental implant integration? *Clin. Oral Implants Res.* **2011**, *22*, 673−680.
(7) Cherian, J. J.; Jauregui, J. J.; Banerjee, S.; Pierce, T.; Mont, M. A. What Host Factors Affect Aseptic Loosening After THA and TKA? *Clin. Orthop. Relat. Res.* **2015**, *473*, 2700−2709.
(8) Kim, K. T.; Eo, M. Y.; Nguyen, T. T. H.; Kim, S. M. General review of titanium toxicity. *Int. J. Implant Dent.* **2019**, *5*, 10.
(9) Isaacson, B.; Jeyapalina, S. Osseointegration: a review of the fundamentals for assuring cementless skeletal fixation. *Orthop. Res. Rev.* **2014**, *6*, 55−65.
(10) Zhao, Q. m.; Xu, G. H.; Hu, A. N.; Xu, R. S.; Jin, H. R. C.; Sun, Y. Y.; Ban, G. F.; Yuan, K.; Zhou, X. G.; Wang, X.; Gui, Z. M. A Mg/Zn-co-doped composite coating on a titanium surface enhances osteogenic activity through the Wnt/beta-catenin pathway. *Appl. Surf. Sci.* **2020**, *515*, 146072.
(11) Wang, J.-Y.; Liu, Y. C.; Lin, G. S.; Chang, H. H.; Li, Y. T.; Yang, Y. C.; Matsuyama, H.; Lee, B. S.; Chen, Y. W.; Tung, K. L. Flame-sprayed strontium- and magnesium-doped hydroxyapatite on titanium implants for osseointegration enhancement. *Surf. Coat. Technol.* **2020**, *386*, 125452.
(12) Zhang, H.; Qiu, J. J.; Liu, X. Y. Enhanced antioxidant capability and osteogenic property of medical titanium by cerium plasma immersion ion implantation. *Surface. Interfac.* **2021**, *26*, 101402.
(13) Kaseem, M.; Fatimah, S.; Nashrah, N.; Ko, Y. G. Recent progress in surface modification of metals coated by plasma electrolytic oxidation: Principle, structure, and performance. *Prog. Mater. Sci.* **2021**, *117*, 100735.
(14) Vu, A. A.; Robertson, S. F.; Ke, D.; Bandyopadhyay, A.; Bose, S. Mechanical and biological properties of ZnO, SiO2, and Ag2O doped plasma sprayed hydroxyapatite coating for orthopaedic and dental applications. *Acta Biomater.* **2019**, *92*, 325−335.
(15) Yu, Y.; Jin, G.; Xue, Y.; Wang, D.; Liu, X.; Sun, J. Multifunctions of dual Zn/Mg ion co-implanted titanium on osteogenesis, angiogenesis and bacteria inhibition for dental implants. *Acta Biomater.* **2017**, *49*, 590−603.
(16) di Giacomo, V.; Cataldi, A.; Sancilio, S. Biological Factors, Metals, and Biomaterials Regulating Osteogenesis through Autophagy. *Int. J. Mol. Sci.* **2020**, *21*, 2789.
(17) Won, E.; Kim, Y. K. An Oldie but Goodie: Lithium in the Treatment of Bipolar Disorder through Neuroprotective and Neurotrophic Mechanisms. *Int. J. Mol. Sci.* **2017**, *18*, 2679.
(18) Minashima, T.; Zhang, Y.; Lee, Y.; Kirsch, T. Lithium protects against cartilage degradation in osteoarthritis. *Arthritis Rheumatol.* **2014**, *66*, 1228−1236.
(19) Pan, C.; Chen, L.; Wu, R.; Shan, H.; Zhou, Z.; Lin, Y.; Yu, X.; Yan, L.; Wu, C. Lithium-containing biomaterials inhibit osteoclastogenesis of macrophages in vitro and osteolysis in vivo. *J. Mater. Chem. B* **2018**, *6*, 8115−8126.
(20) Clément-Lacroix, P.; Ai, M.; Morvan, F.; Roman-Roman, S.; re, B. a. V.; Belleville, C.; Estrera, K.; Warman, M. L.; Baron, R.; Rawadi, G. Lrp5-independent activation of Wnt signaling by lithium chloride increases bone formation and bone mass in mice. *Proc. Natl. Acad. Sci. U.S.A.* **2005**, *102*, 17406.
(21) Liu, W.; Chen, D.; Jiang, G.; Li, Q.; Wang, Q.; Cheng, M.; He, G.; Zhang, X. A lithium-containing nanoporous coating on entangled titanium scaffold can enhance osseointegration through Wnt/beta-catenin pathway. *Nanomedicine* **2018**, *14*, 153−164.
(22) Peng, F.; Qiu, L.; Yao, M.; Liu, L.; Zheng, Y.; Wu, S.; Ruan, Q.; Liu, X.; Zhang, Y.; Li, M.; Chu, P. K. A lithium-doped surface inspires immunomodulatory functions for enhanced osteointegration through PI3K/AKT signaling axis regulation. *Biomater. Sci.* **2021**, *9*, 8202−8220.
(23) Budni, J.; Feijó, D. P.; Batista-Silva, H.; Garcez, M. L.; Mina, F.; Belletini-Santos, T.; Krasilchik, L. R.; Luz, A. P.; Schiavo, G. L.; Quevedo, J. Lithium and memantine improve spatial memory impairment and neuroinflammation induced by beta-amyloid 1-42 oligomers in rats. *Neurobiol. Learn. Mem.* **2017**, *141*, 84−92.
(24) Liu, L.; Liu, Y.; Feng, C.; Chang, J.; Fu, R.; Wu, T.; Yu, F.; Wang, X.; Xia, L.; Wu, C.; Fang, B. Lithium-containing biomaterials stimulate bone marrow stromal cell-derived exosomal miR-130a secretion to promote angiogenesis. *Biomaterials* **2019**, *192*, 523−536.
(25) Deng, C.; Zhu, H.; Li, J.; Feng, C.; Yao, Q.; Wang, L.; Chang, J.; Wu, C. Bioactive Scaffolds for Regeneration of Cartilage and Subchondral Bone Interface. *Theranostics* **2018**, *8*, 1940−1955.
(26) Pavarini, M.; Moscatelli, M.; Candiani, G.; Tarsini, P.; Cochis, A.; Rimondini, L.; Najmi, Z.; Rocchetti, V.; De Giglio, E.; Cometa, S.; De Nardo, L.; Chiesa, R. Influence of frequency and duty cycle on the properties of antibacterial borate-based PEO coatings on titanium for bone-contact applications. *Appl. Surf. Sci.* **2021**, *567*, 150811.
(27) Rafieerad, A. R.; Ashra, M. R.; Mahmoodian, R.; Bushroa, A. R. Surface characterization and corrosion behavior of calcium phosphate-base composite layer on titanium and its alloys via plasma electrolytic oxidation: A review paper. *Mater. Sci. Eng., C* **2015**, *57*, 397−413.
(28) Hussein, R. O.; Nie, X.; Northwood, D. O. An investigation of ceramic coating growth mechanisms in plasma electrolytic oxidation (PEO) processing. *Electrochim. Acta* **2013**, *112*, 111−119.
(29) Ding, Z.; Qiao, Y.; Peng, F.; Xia, C.; Qian, S.; Wang, T.; Sun, J.; Liu, X. Si-doped porous TiO2 coatings enhanced in vitro angiogenic behavior of human umbilical vein endothelial cells. *Colloids Surf., B* **2017**, *159*, 493−500.
(30) Yang, X.; Zhang, C.; Zhang, T.; Xiao, J. Cobalt-doped Ti surface promotes immunomodulation. *Biomed. Mater.* **2022**, *17*, 025003.
(31) Bu, Y.; Wang, X. H.; Li, L. X.; Hu, X. F.; Tan, D. D.; Li, Z. L.; Lai, M. H.; Qiu, X. Z.; Sun, F. F.; Wang, H. F.; Yang, F.; Wu, D. C.; Guo, J. S. Lithium Loaded Octa-Poly(Ethylene Glycol) Based Adhesive Facilitates Axon Regeneration and Reconnection of Transected Peripheral Nerves. *Adv. Healthcare Mater.* **2020**, *9*, 2000268.
(32) Carville, N. C.; Neumayer, S. M.; Manzo, M.; Gallo, K.; Rodriguez, B. J. Biocompatible Gold Nanoparticle Arrays Photodeposited on Periodically Proton Exchanged Lithium Niobate. *ACS Biomater. Sci. Eng.* **2016**, *2*, 1351−1356.
(33) Gulseren, G.; Yasa, I. C.; Ustahuseyin, O.; Tekin, E. D.; Tekinay, A. B.; Guler, M. O. Alkaline Phosphatase-Mimicking Peptide Nanofibers for Osteogenic Differentiation. *Biomacromolecules* **2015**, *16*, 2198−2208.
(34) Sun, D.; Xu, W.; Liang, C.; Shi, W.; Xu, S. Smart Surface-Enhanced Resonance Raman Scattering Nanoprobe for Monitoring Cellular Alkaline Phosphatase Activity during Osteogenic Differentiation. *ACS Sens.* **2020**, *5*, 1758−1767.
(35) Yuan, Y.; Yuan, Q.; Wu, C.; Ding, Z.; Wang, X.; Li, G.; Gu, Z.; Li, L.; Xie, H. Enhanced Osteoconductivity and Osseointegration in

https://doi.org/10.1021/acsomega.2c00229
ACS Omega 2022, 7, 12030−12038

Calcium Polyphosphate Bioceramic Scaffold via Lithium Doping for Bone Regeneration. *ACS Biomater. Sci. Eng.* **2019**, *5*, 5872−5880.
(36) Rutkovskiy, A.; Stensløkken, K.-O.; Vaage, I. J. Osteoblast Differentiation at a Glance. *Med. Sci. Monit. Basic Res.* **2016**, *22*, 95−106.
(37) Clément-Lacroix, P.; Ai, M.; Morvan, F.; Roman-Roman, S.; Vayssière, B.; Belleville, C.; Estrera, K.; Warman, M. L.; Baron, R.; Rawadi, G. Lrp5-independent activation of Wnt signaling by lithium chloride increases bone formation and bone mass in mice. *Proc. Natl. Acad. Sci. U.S.A.* **2005**, *102*, 17406−17411.
(38) Salhotra, A.; Shah, H. N.; Levi, B.; Longaker, M. T. Mechanisms of bone development and repair. *Nat. Rev. Mol. Cell Biol.* **2020**, *21*, 696−711.
(39) Ambrosi, T. H.; Longaker, M. T.; Chan, C. K. F. A Revised Perspective of Skeletal Stem Cell Biology. *Front. Cell Dev. Biol.* **2019**, *7*, 189.
(40) Iwayama, T.; Okada, T.; Ueda, T.; Tomita, K.; Matsumoto, S.; Takedachi, M.; Wakisaka, S.; Noda, T.; Ogura, T.; Okano, T.; Fratzl, P.; Ogura, T.; Murakami, S. Osteoblastic lysosome plays a central role in mineralization. *Sci. Adv.* **2019**, *5*, No. eaax0672.
(41) Kurgan, N.; Bott, K. N.; Helmeczi, W. E.; Roy, B. D.; Brindle, I. D.; Klentrou, P.; Fajardo, V. A. Low dose lithium supplementation activates Wnt/β-catenin signalling and increases bone OPG/RANKL ratio in mice. *Biochem. Biophys. Res. Commun.* **2019**, *511*, 394−397.
(42) Huang, T.-b.; Li, Y.-z.; Yu, K.; Yu, Z.; Wang, Y.; Jiang, Z.-w.; Wang, H.-m.; Yang, G.-l. Effect of the Wnt signal- RANKL/ OPG axis on the enhanced osteogenic integration of a lithium incorporated surface. *Biomater. Sci.* **2019**, *7*, 1101−1116.
(43) Shah, F. A.; Thomsen, P.; Palmquist, A. Osseointegration and current interpretations of the bone-implant interface. *Acta Biomater.* **2019**, *84*, 1−15.
(44) De Fusco, C.; Messina, A.; Monda, V.; Viggiano, E.; Moscatelli, F.; Valenzano, A.; Esposito, T.; Sergio, C.; Cibelli, G.; Monda, M.; Messina, G. Osteopontin: Relation between Adipose Tissue and Bone Homeostasis. *Stem Cell. Int.* **2017**, 4045238.
(45) Icer, M. A.; Gezmen-Karadag, M. The multiple functions and mechanisms of osteopontin. *Clin. Biochem.* **2018**, *59*, 17−24.
(46) Jeon, E. Y.; Baek, S. E.; Kim, J. O.; Choi, J. M..; Jang, E. J.; Kim, C. D. A Pivotal Role for AP-1-Mediated Osteopontin Expression in the Increased Migration of Vascular Smooth Muscle Cells Stimulated With HMGB1. *Front. Physiol.* **2021**, *12*, 775464.
(47) Lee, G. S.; Salazar, H. F.; Joseph, G.; Lok, Z. S. Y.; Caroti, C. M.; Weiss, D.; Taylor, W. R.; Lyle, A. N. Osteopontin isoforms differentially promote arteriogenesis in response to ischemia via macrophage accumulation and survival. *Lab. Invest.* **2019**, *99*, 331−345.

https://doi.org/10.1021/acsomega.2c00229
ACS Omega 2022, 7, 12030−12038